IC/2001/44

united nations
educational, scientific
and cultural
organization

international atomic
energy agency

the
abdus salam
international
centre
for theoretical
physics

TURBULENCE MODELS IN SUPERSONIC FLOWS

E. Shirani

H. Ahmadikia

and

S. Talebi

IC/2001/44

United Nations Educational Scientific and Cultural Organization
and
International Atomic Energy Agency

THE ABDUS SALAM INTERNATIONAL CENTRE FOR THEORETICAL PHYSICS

TURBULENCE MODELS IN SUPERSONIC FLOWS

E. Shirani[1]
Department of Mechanical Engineering, Isfahan University of Technology, Isfahan, Iran
and
The Abdus Salam International Centre for Theoretical Physics, Trieste, Italy,

H. Ahmadikia
Bou-Ali-Sina University, Iran

and

S. Talebi
Yazd University, Yazd, Iran.

Abstract

The aim of this paper is to evaluate five different turbulence models when used in rather complicated two-dimensional and axisymmetric supersonic flows. They are Baldwin-Lomax, k-l, k-ε, k-ω and k-ζ turbulence models. The compressibility effects, axisymmetric correction terms and some modifications for transition region are used and tested in the models. Two computer codes based on the control volume approach and two flux-splitting methods, Roe and Van Leer, are developed. The codes are used to simulate supersonic mixing layers, flow behind axisymmetric body, under expanded jet, and flow over hollow cylinder flare. The results are compared with experimental data and behavior of the turbulence models is examined. It is shown that both k-l and k-ζ models produce very good results. It is also shown that the compressibility correction in the model is required to obtain more accurate results.

MIRAMARE – TRIESTE
May 2001

[1] Regular Associate of the Abdus Salam ICTP. E-mail: eshirani@cc.iut.ac.ir

Nomenclature

e_t	Total energy	Mc	Convective Mach number	V	Free stream velocity
k	Conduction coefficient	M_e	Free stream Mach number	x_t	Transition point
k	Turbulent kinetic energy	p	Pressure	ρ	density
k_τ	Turbulent eddy diffusivity	T	temperature	μ	viscosity
l^t	Turbulent length scale	R_j	Jet radius	μ_τ	Turbulent eddy viscosity
L_{TS}	Tolliman-Shilichting length	U	x-velocity component	ν^*	Viscosity at ref. temperature
L_{SM}	Acoustic length scale	U_e	Free stream velocity		

1.Introduction

1.1 General

Supersonic flows are important in many applications including aerodynamics and turbomachinery. These flows contain several complicated phenomena such as strong curved shock waves and entropy or vorticity layers in front of the body, shock waves/boundary layers interactions, expansion and compression waves, separation and recirculation zones, wake with recirculation regions and reattachment points, mixing layers. The drag force and also the control and stability of a projectile motion depend very much on these phenomena. Thus it is important to simulate these kinds of flows with care. The Reynolds number in high-speed flows around projectile objects is extremely high and turbulence effects are remarkable. The proper way of handling the turbulence phenomena is crucial for the accurate prediction of drag, heat load, inlet efficiency, and stability of the projectile.

Turbulent flow is highly vortical, three-dimensional, and time dependent. It contains a wide range of length scales from as big as the size of the whole domain to as small as the Kolmogrov length scale [1]. In order to resolve all the scales numerically, the size of grid cells must be smaller than the smallest length scale, so one should use a very large number of grid points. A simulation of this kind, which is called direct numerical simulations (DNS), can only be performed on supercomputers for simple flows.

Large eddy simulation technique (LES) is another advanced numerical simulation of the flow. In this technique, the small structures of the flow, which are more or less universal and do not depend on the flow geometric, are modeled by simple relations and the large scales are simulated. The number of the grid points needed for this method is smaller, because we do not need to resolve small scales. Yet, since the large eddies of the turbulent flows are three-dimensional and time dependent, the governing equations must be solved in a three-dimensional, time dependent form. This kind of calculation also needs high-speed large computers.

The most practical way of simulating turbulent flows thus far is by using Reynolds average idea to filter the turbulence fluctuations. In this technique, the Navier-Stokes equations are integrated over a time interval which is larger than the turbulence time scale, but is much smaller than the mean flow time scale. Due to the non-linearity of Navier-Stokes equations, the so-called Reynolds average equations, which resulted from such averaging, have some extra unknown terms, the Reynolds stresses and turbulent heat diffusion. The relation of these quantities in particular with the mean flow variables requires the introduction of some modellization of these unknown relations, based on theoretical considerations coupled to unavoidable empirical information. This information was considered to be contained in the turbulence models, to be added to the averaged Navier-Stokes equations.

Based on Morkovin [2] hypothesis, for compressible flows, the effects of density fluctuation on the turbulence structure will remain small for Mach numbers below 5 for boundary layers and wakes, and below 1.5 for jets, Bradshaw [3]. It implies that the turbulence models, based on density-averaged quantities will remain valid with the empirical data taken from incompressible flow experiments, within these limits of Mach number. Yet in compressible flows, some extra terms such as velocity-pressure correlation are non-zero and must be modeled.

Many different models ranging from simple zero-equation models, algebraic models, to second order closure models have been developed. The most popular turbulence modeling is the first order closure models of Reynolds stresses and mean turbulent heat flux by means of introducing the concept of the eddy viscosity and eddy diffusivity, respectively. This idea is based on the original assumption of Boussinsq [4]. The first order models can be classified

according to the number of additional transport equations for the turbulent quantities they require. The algebraic models do not require any differential equations for the turbulent quantities and are therefore the simplest and easiest models to use. Models using one or two additional differential equations are therefore called one-equation and two-equation models, respectively.
In the second order closure models, transport equations for the second-order correlation, the Reynolds stress and averaged turbulent heat flux, are deduced from the Navier-Stokes equations and the third-order correlation terms appearing in the equations are modeled as a function of the second order correlation. These models are quite general but require the solution of a system of transport equations for each of the second order correlation terms. The computational effort involved is large. The authors believe from their previous experience that this complexity can be avoided for simple flow configurations by using simpler models such as the first order models, which are the center of attention in this paper. These models can provide an approximation of the influence of turbulent transport and diffusion on the mean flow quantities.

1.2. Turbulence Models

In this section, a literature review for the most commonly used turbulence models and some new models, which are all based on the eddy viscosity model, are presented briefly. The focus is on the modifications made for compressible flows and the emphasis is on the models that are used in this paper. By similarity analysis, the eddy viscosity is a function of two variables, turbulent kinetic energy, k and a turbulent length scale, l. In two-equation models, two transport equations, one for k, and the other for φ are solved. φ is used instead of the turbulent length scale. Its general form is $\varphi=k^n\ l^m$. Depending on the values of n and m, φ can be turbulent energy dissipation rate, ε, variance of vorticity fluctuations, or enstrophy, ξ, the ratio of the turbulent energy dissipation rate to the turbulent kinetic energy, ω, or turbulent length scale, l.

a. Baldwin-Lomax model

To the knowledge of authors, The Baldwin-Lomax model [5] is the most successful zero-equation model which was used for compressible turbulent flows. This model is the modified version of Cebeci-Smith's [6] two-layer algebraic model. It is used and adjusted for rather simple flows such as boundary layers and its interaction with shock waves. But due to the existence of different mean flow length scales, it cannot predict the flow accurately in the more complicated flows. Shirazi and Truman [7] have studied this model extensively. They found that the model produces poor results when used for separated flows or flows with complicated geometry. Granville [8] and [9] modified the model for flow with high-pressure gradient and compressibility effects.

b. k-ε model

The majority of the turbulence modeling works that have been done in the last thirty years, correspond to k-ε models. Launder [10] introduced the model in its present form. The k-ε model overestimates the skin friction coefficient when applied to the boundary layer flows with adverse pressure gradient. In the modified k-ε model, a source term is added to the ε equation, to overcome this problem. Sarkar [11] and Zemman [12] have modeled the dilatation dissipation and dilatation pressure using DNS results and applied the k-ε and Reynolds stress models to simulate simple free shear flows and obtained good results.

c. k-ω model

The k-ω equation was recently tackled by more researchers. This model was first used by Spalding [13], and then Wilcox [14] modified it. The k-ω equation is sensitive to free stream boundary conditions. Huang et al. [15] showed that for incompressible flows with adverse pressure gradient, k-ω model produces better results than k-ε. Wilcox and Alber [16] used Favre (density-weighted) averaged model for compressible flows. Rubesin [17] modeled the previously neglected extra compressible term in the k equation. Wilcox and Rubesin [18] have used the modified Wilcox and Tracy model for compressible subsonic flows and got good results. Viegas and Horstman [19] tested several models for supersonic flow over compression corner and showed that the two-equation models of Wilcox and Rubensin [18] and Jones and Launder [20] produce better results compared to zero-equation models. They show that zero-equation models do not predict skin friction accurately, and neither of the models can predict location of separation points accurately.

Like the k-ε model, the k-ω model was also modified according to Sarkar [11], Zemman [12] and Wilcox [21]. Wilcox [22] showed that these modifications are not appropriate for flow over a flat plate. Huang et al. [15] modified k-ε and k-ω models using Zemman [12], Sarkar [11] and Elbaz [23] compressibility correction models. They showed that these modifications are not appropriate for predicting the pure Couette flows.

d. k-l model

Although it seems that the natural way of obtaining two-equation models is to use k-l equations, but the k-l equations has gained much less attention by researchers. Rotta [24] and Spalding [13] have derived a differential transport equation for length scale, l, and applied it successfully to free shear flows. Smith [25] and [26] introduced a transport equation for length scale and applied it to shear flows with success. Ahmadikia [27] derived the k-l model from Saeedi's et al. [28] k-kl model and made some new successful modifications to simulate supersonics flows and transition region. Some of the results will be presented in this paper.

e. k-ζ model

In this model, ζ is very similar to ε, but in the ε equation, all the terms associated to the large scale of the flow are eliminated, whereas in the ζ equation, those terms are modeled. So it is expected that the k-ζ model produces a better result especially when the local Reynolds number is small because in this case the small scales are not mean flow independent. Robinson and Hassan [29] in 1995 introduced the k-ζ model for incompressible flows. They applied the model for free shear layers in their paper. Later the model was applied to simulate boundary layers, compressible shear flows, near wall correction, separated flows and three-dimensional compressible flows by Robinson and Hassan [30], Alexopoulos and Hassan, [31], Robinson and Hassan [32], [33], and [34], respectively. More recently, Talebi [35] applied the model for more complicated compressible flows. Some of his results will be presented in this paper.

2. Governing Equations

Two-dimensional axisymmetric, compressible Reynolds averaged Navies-Stokes equations, which are numerically solved in this paper, are as follow:

$$\frac{\partial \vec{Q}}{\partial \tau}+\frac{\partial \vec{E}_i}{\partial x}+\frac{\partial \vec{F}_i}{\partial y}=\frac{\partial \vec{E}_v}{\partial x}+\frac{\partial \vec{F}_v}{\partial y}+\vec{H} \tag{1}$$

where,

$$\vec{Q}=y^m\begin{bmatrix}\rho\\ \rho u\\ \rho v\\ e_t\\ \rho k\\ \rho\phi\end{bmatrix} \qquad \vec{E}_i=y^m\begin{bmatrix}\rho u\\ \rho u^2+p+\frac{2}{3}\rho k\\ \rho uv\\ \left(e_t+p+\frac{2}{3}\rho k\right)u\\ \rho uk\\ \rho u\phi\end{bmatrix} \qquad \vec{F}_i=y^m\begin{bmatrix}\rho v\\ \rho uv\\ \rho v^2+p+\frac{2}{3}\rho k\\ \left(e_t+p+\frac{2}{3}\rho k\right)v\\ \rho vk\\ \rho v\phi\end{bmatrix}$$

$$\vec{E}_v=y^m\begin{bmatrix}0\\ \tau_{xx}\\ \tau_{xy}\\ u\tau_{xx}+v\tau_{xy}+\dot{q}_x\\ -\dot{q}_{kx}\\ -\dot{q}_{\phi x}\end{bmatrix} \qquad \vec{F}_v=y^m\begin{bmatrix}0\\ \tau_{yx}\\ \tau_{yy}\\ u\tau_{xy}+v\tau_{yy}+\dot{q}_y\\ -\dot{q}_{ky}\\ -\dot{q}_{\phi y_i}\end{bmatrix} \qquad \vec{H}=\begin{bmatrix}0\\ 0\\ m(p-\tau_{\theta\theta})\\ 0\\ y^m H_k\\ y^m H_\phi\end{bmatrix}$$

$$\tau_{xx}=(\lambda+2\mu_t)\frac{\partial u}{\partial x}+\lambda\left(\frac{\partial v}{\partial y}+m\frac{v}{y}\right) \qquad \tau_{xy}=\mu_t\frac{\partial u}{\partial x}+\left(\frac{\partial u}{\partial y}+m\frac{v}{y}\right) \tag{2}$$

$$\tau_{yy}=(\lambda+2\mu_t)\frac{\partial v}{\partial y}+\lambda\left(\frac{\partial u}{\partial x}+m\frac{v}{y}\right) \qquad \tau_{\theta\theta}=(\lambda+2\mu_t)\frac{v}{y}+\lambda\left(\frac{\partial u}{\partial x}+\frac{\partial v}{\partial y}\right)$$

$$\lambda=-\frac{2}{3}\mu \tag{3}$$

$$\dot{q}_x=-(k+k_\tau)\frac{\partial T}{\partial x} \qquad \dot{q}_y=-(k+k_\tau)\frac{\partial T}{\partial y} \tag{4}$$

$$\dot{q}_{\phi x}=-\left(\mu+\frac{\mu_\tau}{\sigma_\phi}\right)\frac{\partial \phi}{\partial x} \qquad \dot{q}_{\phi y}=-\left(\mu+\frac{\mu_\tau}{\sigma_\phi}\right)\frac{\partial \phi}{\partial y} \tag{5}$$

$$k_\tau=\mu_\tau c_p/\mathrm{Pr}_\tau, \qquad \mathrm{Pr}_\tau=0.9, \qquad \mu_t=\mu+\mu_\tau \tag{6}$$

where, m is equal to one for axisymmetric flows and is zero for two-dimensional flows, and ϕ is a dummy variable and may be ε, ω, ξ, or l depending on which model is used.

3. Turbulence Model Equations

As mentioned earlier, five different turbulence models are used in this paper. The models are as follows:

3.1 Baldwin-Lomax Model

The algebraic Baldwin-Lomax model is based on the eddy viscosity model and consists of two layers. In the inner layer, the eddy viscosity is obtained from Prandtl mixing length and Van Drist damping function.

$$\mu_{ti} = \rho \ell^2 |\omega|, \qquad \ell = \kappa y (1 - e^{-y^+/A^+}) \tag{7}$$

$$\mu_{t0} = K C_{cp} \rho F_{kleb}(y), \qquad F_{kleb} = y_{\max} F_{\max}, \qquad F_{\max} = \max[F(y)] = \max\left[|\omega| y (1 - e^{-y^+/A^+})\right] \tag{8}$$

$$F_{kleb} = \left[1 + 5.5 (C_{kleb} y / y_{\max})^6\right]^{-1} \tag{9}$$

y_{max} is the location where F is maximum, $\omega = u_y - u_x$, κ=0.41, K=0.168, $C_{cp} = 1.6$ and A^+=26.

To improve the algebraic turbulence models, the eddy viscosity at the wake region is modified as follows:

$$\mu_\tau = \mu_{\tau,\max} \left(\frac{\omega}{\omega_{\max}} \right)^n \tag{10}$$

where, $\mu_{\tau,\max}$ and $\omega_{\max}$ are the maximum values of μ_τ and ω_τ at the center of the body and n=0.15.

3.2 k-ε model

The k-ε model based on Chain near wall correction [36], and Sarkar [11] and Zemman [12] compressibility corrections, are:

$$\frac{\partial \rho k}{\partial t} + \frac{(\partial \rho k u_j)}{\partial x_j} = \frac{1}{r^m} \frac{\partial}{\partial x_j} \left[\left(\mu + \frac{\mu_\tau}{\sigma_k} \right) \frac{\partial k}{\partial x_j} \right] + P_k - \rho(\tilde{\varepsilon} + \varepsilon_0) + \pi_{c1} + \pi_{c2} + \pi_{c3} \tag{11}$$

$$\frac{\partial (\rho \tilde{\varepsilon})}{\partial t} + \frac{\partial (\rho \tilde{\varepsilon} u_j)}{\partial x_j} + = \frac{1}{r^m} \frac{\partial}{\partial x_j} \left[\left(\mu + \frac{\mu_\tau}{\sigma_\varepsilon} \right) \frac{\partial \tilde{\varepsilon}}{\partial x_j} \right] + C_{\varepsilon 1} f_{\varepsilon 1} P_k \frac{\tilde{\varepsilon}}{k} - C_{\varepsilon 2} f_{\varepsilon 2} \rho \frac{\tilde{\varepsilon}^2}{k} + S_\varepsilon + S_{\varepsilon c} \tag{12}$$

$$\mu_\tau = f_\mu C_\mu \rho k^2 / \tilde{\varepsilon}, \qquad \tilde{\varepsilon} = \varepsilon - \varepsilon_0 \tag{13}$$

$$P_k = \frac{1}{2} \mu_\tau \left(\frac{\partial u_i}{\partial x_j} + \frac{\partial u_j}{\partial x_i} \right) \left(\frac{\partial u_i}{\partial x_j} + \frac{\partial u_j}{\partial x_i} - \frac{2}{3} \frac{\partial u_j}{\partial x_j} \delta_{ij} \right) - \frac{1}{3} \rho k \left(\frac{\partial u_i}{\partial x_j} + \frac{\partial u_j}{\partial x_i} \right) \delta_{ij} \tag{14}$$

$C_{\varepsilon 1} = 1.44$, $C_{\varepsilon 2} = 1.92$, $C_\mu = 0.09$, $\sigma_k = 1$, $\sigma_\varepsilon = 1.3$

where, in both k-ε and k-ω models, ε_0, f_μ, $f_{\varepsilon 1}$, $f_{\varepsilon 2}$ are given in [36] and the source terms π_{c1}, π_{c2}, π_{c3} are given in [11] and [12].

3.3 k-ω model

The equations for k and ω with Wilcox near wall correction, and Sarkar [11] and Zemman [12] compressibility corrections used by Wilcox [18], are:

$$\frac{\partial (\rho k)}{\partial t} + \frac{\partial (\rho k u_j)}{\partial x_j} = \frac{1}{r^m} \frac{\partial}{\partial x_j} \left[\left(\mu + \frac{\mu_\tau}{\sigma_k} \right) \frac{\partial k}{\partial x_j} \right] + P_k - \beta_0^* \rho \omega k f_1 + \pi_{c1} + \pi_{c2} + \pi_{c3} \tag{15}$$

$$\frac{\partial(\rho\omega)}{\partial t}+\frac{\partial(\rho\omega u_j)}{\partial x_j}=\frac{1}{r^m}\frac{\partial}{\partial x_j}\left[\left(\mu+\frac{\mu_\tau}{\sigma_\omega}\right)\frac{\partial\omega}{\partial x_j}\right]+\alpha\frac{\omega}{k}P_k f_2-\beta_0\rho\omega^2 \tag{16}$$

$$\mu_\tau=f_\mu C_\mu \rho k/\omega \tag{17}$$

$$C_\mu=1\quad,\quad \beta_0=0.075\quad,\quad \beta_0^*=0.09\quad,\quad \alpha=0.56\quad,\quad \sigma_k=2\quad,\quad \sigma_\omega=2$$

3.4 k-l model

The final form of the modified k-l equations and their constants, according to Ahmadikia [27], are:

$$\frac{\partial\rho k}{\partial t}+\frac{(\partial\rho k u_j)}{\partial x_j}=\rho P_k-c_D\rho\frac{k^{3/2}}{\ell}+\frac{\partial}{\partial x_k}\left[(\mu+\mu_\tau/\sigma_k)\frac{\partial k}{\partial x_k}\right]-\mu\frac{\partial k}{\partial x_i}\frac{\partial k}{\partial x_i} \tag{18}$$

$$\frac{\partial\rho\ell}{\partial t}+\frac{\partial\rho(\ell u_j}{\partial x_j}=C_L\rho k^{1/2}+\frac{\partial}{\partial x_k}\left[(\mu+\mu_\tau/\sigma_L)\frac{\partial\ell}{\partial x_k}\right]+\rho\ell\frac{\partial u_i}{\partial x_i}+2(\mu+\mu_\tau/\sigma_L)\frac{\partial\ell}{\partial x_i}\frac{\partial k}{\partial x_i} \tag{19}$$

$$\mu_\tau=C_\mu\rho\sqrt{k}\ell,\quad P_k=-\overline{u_i'u_j'}\frac{\partial u_i}{\partial x_j},\quad -\overline{u_i'u_j'}=\nu_t\left(\frac{\partial u_i}{\partial x_j}+\frac{\partial u_j}{\partial x_i}\right)-\frac{2}{3}\delta_{ij}k \tag{20}$$

$$C_L=0.034,\qquad C_D=0.085,\qquad C_\mu=1,\qquad \sigma_k=\sigma_L=1.2$$

The compressibility corrections [26], are:

$$\mu_\tau'=\mu_\tau\frac{1}{(\alpha^2+r^2)^{1/2}} \tag{21}$$

$$\alpha=0.9989,\quad r^2=\frac{3\mu_\tau^2 S_{ij}S_{ij}}{8\ \rho^2k^2},\quad S_{ij}=\left(\frac{\partial u_i}{\partial x_j}+\frac{\partial u_j}{\partial x_i}\right)-\frac{2}{3}\left(\frac{\partial u_k}{\partial x_k}\right)\delta_{ij} \tag{22}$$

and the modifications for transition region, Warren et al [37], are:

$$\ell_\mu=C_D\left[(1-\Gamma)(\ell_{TS}+\ell_{SM})+\Gamma\ell_\mu^t\right] \tag{23}$$

$$\Gamma(x)=1-\exp\left(-0.412\xi^2\right),\quad \xi=(x-x_t)/\lambda,\quad \mathrm{Re}_\lambda=9(\mathrm{Re}_{xt})^{0.75} \tag{24}$$

$$\ell_{TS}=a\sqrt{k/\omega},\quad \ell_{SM}=\frac{b}{U_P}M_e^2\sqrt{\frac{kx}{\mathrm{Re}_x}},\quad \omega\nu^*/U_e^2=3.2\left(\mathrm{Re}_\delta^*\right)^{-2/3} \tag{25}$$

where, $C_D=0.09$, a=0.04-0.06, b=0.23, $U_P=0.94U_e$.

3.5 k-ζ model

The modeled k-ζ equations, according to Robinson and Hassan [34], are:

$$\frac{\partial(\rho k)}{\partial t}+\frac{\partial(\rho k u_j)}{\partial x_j}=\frac{\partial}{\partial x_j}\left[\left(\frac{\mu}{3}+\frac{\mu_\tau}{\sigma_k}\right)\frac{\partial k}{\partial x_j}\right]+\frac{\partial u_i}{\partial x_j}t_{ij}-\mu\zeta-c_1\frac{\rho k}{\tau_\rho}-\frac{\mu_\tau}{c_k\rho^2}\frac{\partial\rho}{\partial x_i}\frac{\partial p}{\partial x_i} \tag{26}$$

$$\frac{\partial(\rho\zeta)}{\partial t}+\frac{\partial(\rho\zeta u_j)}{\partial x_j}=\mu\frac{\partial^2\zeta}{\partial x_i\partial x_i}-2\rho\zeta S_{ii}+\pi_1+\pi_2+\pi_3+\pi_4+\pi_5+\pi_6+\pi_7+\pi_8 \tag{27}$$

where, the correction in the fourth term on the right-hand side of k equation is due to the axisymmetric effects and :

$$\frac{1}{\tau_\rho}=\frac{1}{\rho}\sqrt{\left(\frac{\bar{V}\times\nabla\rho}{V}\right)^2}\,k \tag{28}$$

The other terms in the equations of ζ are modeled as:

$$\pi_1=\frac{1}{\sigma_R}\Omega_{i,j}\left[(\mu\Omega_i)_{,j}+(\mu\Omega_j)_{,i}\right]+\varepsilon_{mij}\Omega_{i,j}\left(t_{mk,k}+\rho k_{,m}\right) \qquad \pi_2=\frac{1}{\sigma_\zeta}\left(\mu\zeta_{,i}\right)_{,i}$$

$$\pi_3=-\beta_7\rho\frac{\Omega_i\Omega_j}{\Omega^2}S_{ij}, \quad \Omega^2=\Omega_i\Omega_i \qquad \pi_4=-\beta_5\rho\frac{\zeta^{1.5}}{\sqrt{\mathrm{Re}_t+\delta}}, \quad \mathrm{Re}_t=\frac{1}{\zeta}\left(\frac{\rho k}{\mu}\right)^2$$

$$\pi_5=\rho\zeta\left(\alpha_3 b_{ij}+\tfrac{2}{3}\delta_{ij}\right)S_{ij}, \quad b_{ij}=\frac{t_{ij}}{\rho k}+\tfrac{2}{3}\delta_{ij}$$

$$\pi_6=-\beta_4\frac{\zeta t_{ij}\Omega_i\Omega_j}{k\Omega}-2\beta_6\frac{t_{ij}}{k}\frac{\mu_\tau}{\mu}\Omega\Omega_i\Omega_j+2\beta_8\frac{t_{ij}}{k}\varepsilon_{imn}k_{,n}\zeta_{,m}\frac{\Omega_j}{S_{ij}S_{ij}+0.5\Omega^2}$$

$$\pi_7=-c_\zeta\rho\sqrt{2\zeta}\frac{\Omega}{2\tau_\rho}$$

$$\pi_8=Max\left[0,\frac{\rho^2 k\Omega}{\mu\sigma_p P}\frac{p_{,t}+u_i p_{,i}}{1+\frac{\sigma_\rho}{\tau_\rho}\sqrt{\frac{\mathrm{Re}_t}{\zeta}}}\right]$$

c_μ is equal to 0.09 and the other constants are given in table (1).

Table 1. Constants for $k-\zeta$ model

c_1	0.6	β_5	2.37	σ_ζ	0.685
$c_{\zeta 1}$	1.35 [31], 2.1 [34]	β_6	0.1	σ_R	0.5
c_k	20	β_7	0.75 [30], 1.5[34]	σ_p	0.13
α_3	0.35	β_8	1.15	σ_ρ	80.0
β_4	0.42	σ_k	0.555	δ	0.1

4. Numerical Solution

The governing equations are transferred into a body fitted coordinate system, and solved numerically. The equations of motion are linearized using the Newton approach and discretized by the control volume approach. Two different codes were prepared. The first one

used the Reimann Roe [38] flux splitting method. In this method, the convective fluxes are approximated by Reimann Roe's method, and diffusion fluxes approximated by second-order central difference scheme. To prevent entropy deflection around the sonic lines, Harten and Hyman [39] entropy conditions are used. To prevent numerical oscillations, the minimum of two-gradient limiter is employed, Hirsh [40]. The second code used the Van Leer [41] flux splitting method. The fluxes at the surfaces of the control volume were approximated by second order accurate method and in order to prevent oscillations around the shock waves or any other large gradient regions, the Koren [42] limiter was used. Finally the equations were solved by using the ADI method. The computational grid is generated algebraically by using the Eiseman method [43].

5. Results

The computer codes were tested with several simple flows to ensure that they worked properly. The results of the testing of the first code are presented by Ahmadikia and Shirani [44]. This code was first used to simulate laminar flow with several different limiter and entropy conditions. The results were compared with experimental data. As a result, the minimum two-gradient limiter and Harten and Hyman [39] entropy condition, which produced better results for the cases studied, were chosen and used in this paper. Simulating channel flow with circular bump and shock tube were used to test the second code. The grid study in both codes was also done. Finally the following five supersonic turbulent flows were simulated and Baldwin-Lomax, k-l, k-ε, k-ω and k-ζ models turbulence models were tested. The first and last cases below were simulated by the second code and the other two cases were simulated by the first code.

5.1 Mixing Layers

In this flow k-ε and k-ζ were used and tested to simulate the flow. The flow conditions were used to simulate a supersonic mixing layer are M_1=1.96, M_2=0.37, M_c=0.64, u_2/u_1=0.25, $T_{o1}=T_{o2}$=276K, ρ_2/ρ_1=0.58, $p_1=p_2$=100KPa.

Fig. (1) shows the velocity distribution and Fig. (2) shows the turbulent kinetic energy. Although the mean velocity distribution are close to the experimental data [45], but the turbulent kinetic energy in k-ε is inaccurate. When the compressibility effects are added to the models, the results for k-ε are closer to the experimental data. But the k-ζ model results are closer to the experimental results. Table (2) indicates the results for different models. As shown in the figures and the table, the k-ζ model produces much better results than the k-ε model. Among the k-ε models, Sarkar compressibility correction produces better results.

Table 2. Relative differences between present results and experimental [45] results (in percent),

	Spreading rate	Reynolds stress	Turbulent kinetic energy
k-ε without correction	17	39	90
k-ε with Sarkar correction	5	16	17
k-ε with Zemman correction	6.5	16	61
k-ε with Wilcox correction	2.5	16	75
k-ζ model	2	4	10

5.2 Flow Behind Axisymmetric Body

Flow behind an axisymmetric body with diameter of 6.35 cm have been simulated using and Baldwin-Lomax, k-ε, k-ω and k-l models and the results compared with the data obtained by Herrin and Duttin [46]. The inflow properties are M_∞ =2.46, T_0 =294K, p_0 = 515 kPa and the free stream turbulent intensity is one percent of free stream velocity. In this case 120×70 grid points were used. Fig. (3) shows the Mach number contours. As shown, the algebraic turbulence model does not produce good results. It shows that a shock wave is present in the wake region, while neither the experimental results nor the numerical simulation obtained from two-equation models produce such shock wave.

The flow configuration and the location of reattachment point shows that k-l and k-ε models produce better results and are closer to the experimental results compared to the k-ω and Baldwin-Lomax models.

The axial velocity along the axis of symmetric is shown in Fig. (4). The locations of reattachment point that are calculated by k-ε and k-ω models are 2.9 and 1.9 percent less than the experimental results respectively. These values are 1.9 and 31 percent of the experimental results when k-l and algebraic models were used, respectively.

Fig. (5) shows the results when the modified version of Baldwin-Lomax model, eq. (10), was used. The results were compared with the original Baldwin-Lomax model. As shown with this modification, much better results, especially for the location of the reattachment point, are obtained.

5.3 Under-expanded Supersonic Jet

In this example, an under-expanded supersonic jet is simulated and k-ε and k-ξ models were tested. The flow conditions are R_j=25mm, M_j=2, $T_{0j}=T_\infty$=293K, T_j=163K, p_∞=10135Kpa, p_j/p_∞=1.45, $R_2=8R_j$, and the number of grid points 39000. Since the jet pressure is smaller than the ambient pressure, a series of shock and expansion waves are produced. The waves are confined in the supersonic region. Fig. (6) shows the density contours, when the k-ε is used. As mixing layer grows, the expansion and shock waves become weaker because of viscosity effect. Fig. (7) compares the pressure distribution on the centerline using k-ε model and the Seiner's experimental data [17] and [18]. When the k-ζ model is used, Fig (8), better results are obtained.

Fig. (9) compares the results obtained from the k-ε model with and without compressibility correction. As shown, when the compressibility effects are neglected in the model, the mixing layer grows faster and the shock waves are damped in shorter distance. Fig. (10) shows the distribution of Mach number as a function of radius at different axial locations. These results are obtained using k-ε and k-ζ models and compared with the experimental data. The results also indicate that the k-ζ model produces much more accurate data. Finally, Fig. (11) shows the x-component of turbulence intensity at $R=R_j$, with different models and compared with the experimental data. The results show that the k-ζ model is the most accurate model. It can also be seen (not shown here) that Sarkar modifications are better than Wilcox's.

5.4 Flow over Hollow Cylinder Flare

In this flow, which shock waves and boundary layers interact, Baldwin-Lomax, k-ω and k-l models are employed and tested. Fig. (12) shows the corresponding geometry and the inflow conditions. The grid size is 160×60. Fig. (13) shows pressure contours in the region near the corner. These results are obtained for k-l model. It shows the locations of separation point, reattachment point, separated region and shock waves. The simulated surface pressure distributions obtained by three different models and also corresponding experimental results

obtained by Joulot [47] are shown in Fig. (14). It shows that the modifications made in k-l equations based on the Warren et al. [37] ideas, produce good results and predict the location of separation point and distribution of pressure well.
Fig. (15) shows the distribution of Stanton number obtained by using three different models and compared with experimental [47] and others numerical [48] data. As shown in Fig. (15), all three models predict the Stanton number well at the transition region and the separation point. But the Baldwin-Lomax model gives less accurate results as expected.
The difference between the numerical results and the experimental ones may be due to the shortcoming of the turbulence models. But it could also be due to the three-dimensionality and unsteadiness nature of the problem, numerical method especially with the use of limiters, grid configuration and the large value of the y^+ on the first node near the wall at the separation region.

6. Conclusions

In this work, five different turbulent models were tested in rather complicated supersonic flows with different flow characteristics and phenomena and the results were compared with experimental data. The two new equations, k-ζ and k-l models, specially the k-ζ model, give better results than the other models. But the k-ζ model is a complicated model with many constants in it. The k-l model is simpler and easier to work with, and it is a promising two-equation model. The compressibility corrections in the models are needed to get better results.

Acknowledgments

This work was done within the framework of the Associateship Scheme of the Abdus Salam International Centre for Theoretical Physics, Trieste, Italy.

References

[1] Kolmogrov , C. R., "The Local Structure of Turbulent in Incompressible Viscous Flow for Very Large Reynolds Number," Dokl. Akad Navk SSSR 30: 301, 538, 1941

[2] Morkovin, M.V., "Effects of Compressibility on Turbulent Flow," In a Favre (ed.), THE MECHACICS OF Turbulence, N.Y., Gordon and Beach, 1964.

[3] Bradshaw, P., "Compressible Turbulent Shear Flows," Annual Review of Fluid Mechanics, **9**, 33-54, 1977.

[4] Boussinsq, J., Theorie de l' Ecoulement Tourbillonant," Vol. 23, pp. 46-50, Paris: Comptes-Rendus de l' Academie des Sciences, 1877.

[5] Baldwin, B. S. and Lomax, H., "Thin layer approximation and algebraic model for separated turbulent flow," AIAA Paper, 78-257, 1978.

[6] Cebeci, T. and Smith, A. M. O., *Analysis of Turbulent Boundary Layers,* Academic, New York, pp. 92-94, 215-217, 1974.

[7] Shirazi, S. A. and Truman, C. R., "Simple turbulence models for supersonic flows: Bodies at Incidence and Compression Corner," AIAA Journal, Vol. 29, No. 11, pp. 1850-1859, 1991.

[8] Granville, P. S., "Baldwin-Lomax factors for turbulent boundary layers in pressure gradient," AIAA Journal, Vol. 25, No. 12, pp. 1624-1627, 1987.

[9] Granville, P. S., " A modified Van Driest formula for the mixing length of turbulent boundary layer in pressure gradient", Journal of Fluid Engineering, Vol. 27, No. 1, pp. 94-97, 1989.

[10] Launder, B. E., Reynolds, W. C., and Rodi, W., *Turbulence Models and their Applications*, Vol. 2, Eyrolls, 1984.

[11] Sarkar, S., "The pressure-dilatation correction in compressible flows," Physics of Fluids, Vol. 4, No. 12, pp.2674-2682, 1992.

[12] Zemman, O., "Dilatation dissipation: The concept and application in model compressible mixing layers," Physics of Fluid, No. 2, pp. 178-188, 1990.

[13] Spalding, D. B., "The calculation of length scale of turbulence in some turbulent boundary layers remote from walls," Imperial College, Heat Transfer Section, Rep TWF/TN/31, 1967.

[14] Wilcox, D .C., "Reassessment of the scale-determining equations of advanced turbulence models," AIAA Journal, Vol. 26, No. 11, pp. 1299-1310, 1988.

[15] Huang, P. G., Bradshaw, P. and Coakley, T. J., "Skin friction and velocity profile family for compressible turbulent boundary layers," AIAA Journal, Vol. 31, No. 9, pp. 1600-1604, 1993.

[16] Wilcox, D. C. and Alber, I. E., "A turbulence model for high speed flows," Proceeding of the 23rd Heat Transfer and Fluid Mechanics, Institute Northridge Cal., pp. 231-252, June 1972.

[17] Rubesin, M. W., "A one-equation model of turbulence for use with the compressible shear layer," AIAA Journal, Vol. 29, No.5, pp. 743-749, 1991.

[18] Wilcox, D. C., and Rubesin, M. W., "Progress in turbulence modeling for complex flow fields including effects of compressibility," NASA, N80-20527, 1980.

[19] Viegas, J. R. and Horstman, C. C., "Comparison of multi equation turbulence models for several shock-boundary layer interaction flows," AIAA Journal, Vol. 17,No. 8, pp. 811-820, 1979.

[20] Jones, W. P. and Launder, B. E., "The prediction of laminarization with two-equation model of turbulence," International Journal of Heat and Mass Transfer, Vol. 15, pp. 301-314, 1972.

[21] Wilcox, D. C., "Progress in hypersonic turbulence modeling," AIAA Paper, 91-1785, 1991.

[22] Wilcox, D. C., "Dilatation-dissipation correction for advanced turbulence models," AIAA Journal, Vol.30, NO. 11, pp. 2639-2646, 1992

[23] Elbaz, A. M., "Modeling compressibility effects on free turbulent shear flow," UMIST, May 1992.

[24] Rotta, J. C., "Statistishe theorie nichthomogener turbulenz," Zeitschrift fur Physik, Vol. 129, pp. 547-572, 1951.

[25] Smith, B. R., "The $k-k\ell$ turbulence model and wall and wall layer model for compressible flows," AIAA Paper, 90-1483, June 1990.

[26] Smith, B. R., "Prediction of hypersonic shock wave turbulent boundary-layer interaction," Journal of Spacecraft and Rockets, Vol. 33, No. 5, 1996.

[27] Ahmadikia, H., "A turbulence Model Based on Length Scale for High-Speed Compressible Axisymmetric Flows," Ph.D. Thesis, Isfahan University of Technology, M.E. Depart., Iran, 2000.

[28] Saeedi, A., Farshchi, M. and Farhanieh, B., "Study of length scale in turbulence modeling,", Sharif Univ., Iran, M.Sc. thesis, 1995.

[29] Robinson, D.F. and Hassan H.A., "Unified Turbulence ClosureModel for Axisymmetric and Plannar Free shear Flows", AIAA Journal, Vol. 33, pp. 2325-2331, 1995.

[30] Robinson, D.F. and Hassan H.A., "A two-equation Turbulence ClosureModel for Wall Bounded and Free Shear Flows," AIAA paper 96-2057, 1996.

[31] Alexopoulos, G.A., and Hassan H.A., "A k-ζ Compressible Turbulence Model for Mixing Layers and Bounded Flows," AIAA paper 96-2039, 1996.

[32] Robinson, D.F. and Hassan H.A., " Modeling Turbulence without Damping Functions Using k-ζ Model,"AIAA paper 97-2312, 1997

[33] Robinson, D.F. and Hassan H.A., "Modeling of Separated Turbulent Flows ,"AIAA paper 97-0207, 1997.

[34] Robinson, D.F. and Hassan H.A., "Further Development of the k-ζ Turbulence Closure Model ,"AIAA Journal, Vol. 36, pp.1825-1833, 1998.

[35] Talebi S., "Simulation of a Super sonic Jet Plume," Ph.D. Thesis, Isfahan University of Technology, M.E. Dept., Iran, 2001.

[36] Chain, K. Y., "Predictions of channel and boundary-layer flows with a low-Reynolds-number turbulence model," AIAA Journal, Vol.20, No. 1, pp.33-38, 1982.

[37] Warren, E.S., Hariss, J.E. and Hassan, H.A., "Transition model for high-speed flow," AIAA Journal, Vol.33, No.8, pp. 1391-1397, 1995.

[38] Roe, P. L., "Characteristic-based schemes for the Euler equations," Annual Review of Fluid Mechanics, Vol. 18, pp. 337-365, 1986.

[39] Harten, A. and Hyman, J. M., "Self adjusting grid methods for one-dimensional hyperbolic conservation Laws," Journal of Computational Physics, Vol. 50, pp. 235-269, 1983.

[40] Hirsh, C., *Numerical Computation of Internal and External Flows,* John Wiley & Sons, New York, Vol.2, 1992.

[41] Van Leer, B., "Flux Vector Splitting for the Euler Equations," Proc. Eighth International Conference on Numerical Methods in Fluid Dynamics, Berlin, Spring Verlag, 1982

[42] Koren, B., "Upwind Schemes, Multigrid and Defect Correction for Steady Navier-Stokes Equations, "Proc. Of Eleventh International Conference on the Numerical Simulation Waves, Berlin, Spring Verlag, 1989

[43] Eiseman, P. R., "A multi-surface method of coordinate generation," Journal of Computational Physics, Vol. 33, pp. 118-150, 1970.

[44] Ahmadikia, H. and Shirani, E., "Assessment of Roe's Reimann solver in hypersonic 2-D and axisymmetric blunt body flows," Journal of Engineering Esteghlal, IUT, Iran, 2001.

[45] Samimy, M., Elliott, G.S., "Effects of Compressibility on the Characteristics of Free Shear Layers," AIAA Journal, Vol. 28, pp. 439-445, 1990.

[46] Herrin, J. L. and Duttin, J. C., "Supersonic base flow experiments in the near wake of a cylindrical afterbody," AIAA Journal, Vol. 32, No. 1, pp.77-83, 1994.

[47] Joulot, A., "Contribution a petude de interaction onde de choc-couche limite sur rampe bidimensionnelle en regime hypersonique," Ph.D. Thesies, Univ. Pierre et Marie Curie, Paris, 1992.

[48] Paciorri, R., Dieudonne, W., Degrez, G., Chabonnier, J.M. and Deconinck, H., "Exploring the validity of the Spalart-Allmars turbulence model for hypersonic flows," Journal of Spacecraft and Rockets, Vol. 35, No. 2, pp. 121-126, 1998.

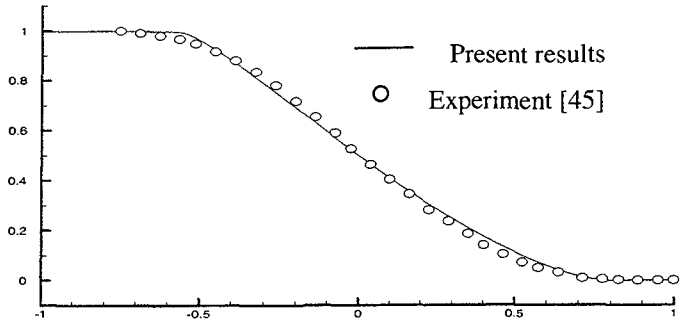

Figure 1. Mean velocity distribution

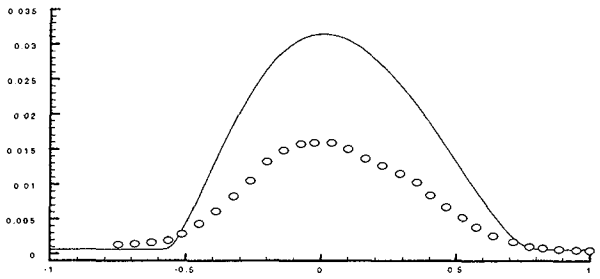

a) k-ε without compressibility correction

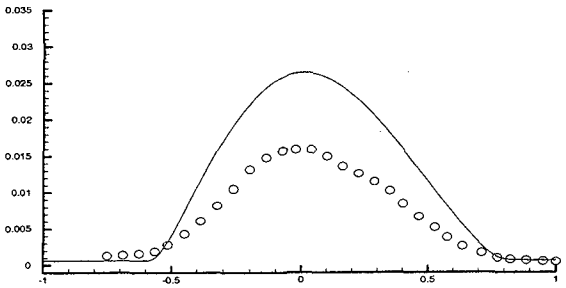

b) k-ε with Sarkar compressibility correction

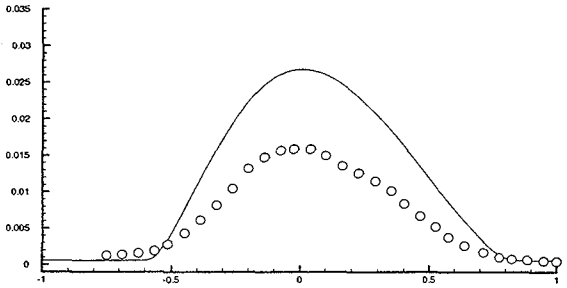

c) k-ε with Zemman compressibility correction

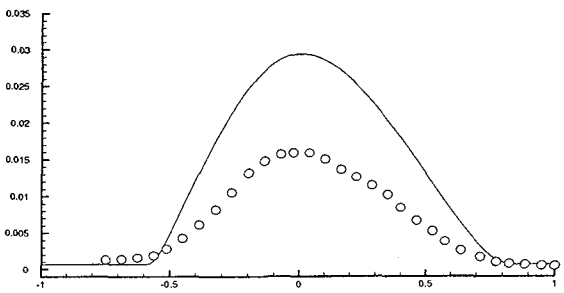

d) k-ε with Wilcox compressibility correction

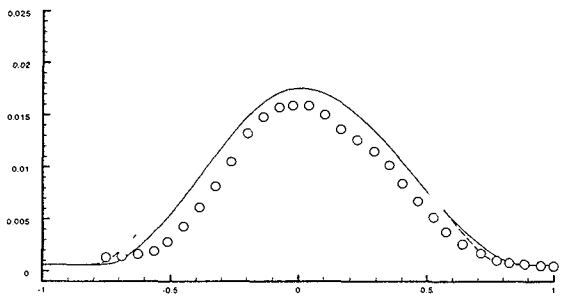

e) k-ζ model

Figure 2. Turbulent kinetic energy

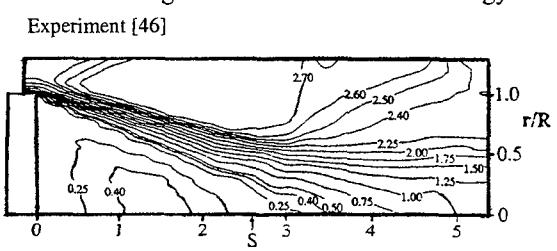

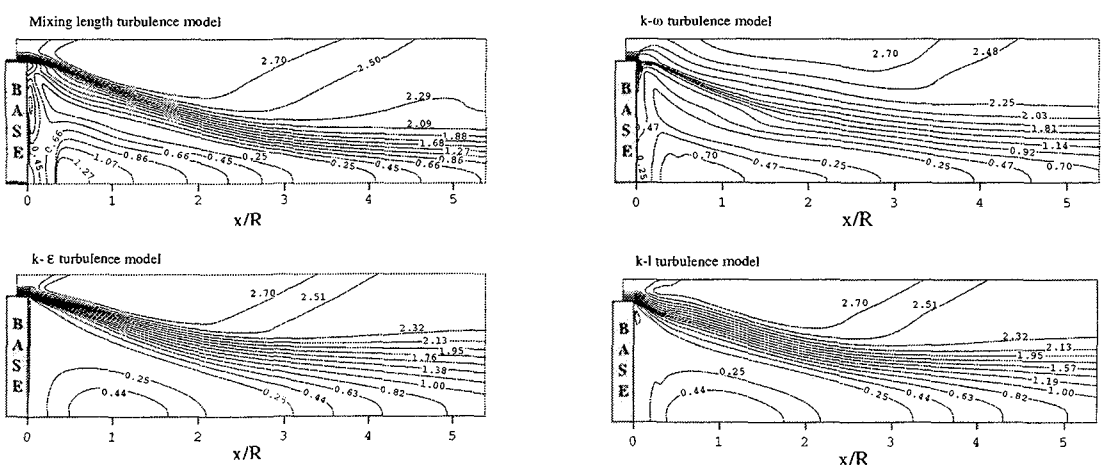

Figure 3. Mach number contours

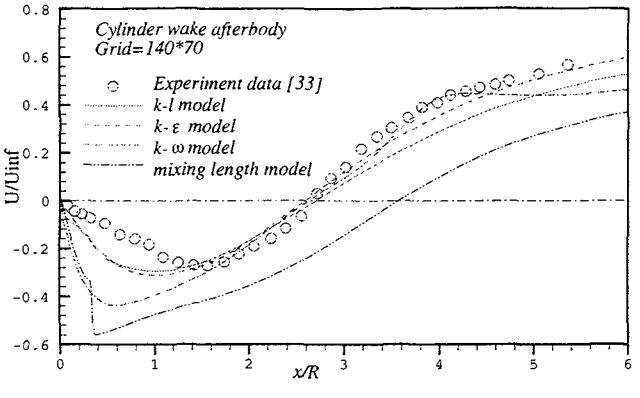

Figure 4. Mean axial velocity along cylinder centerline

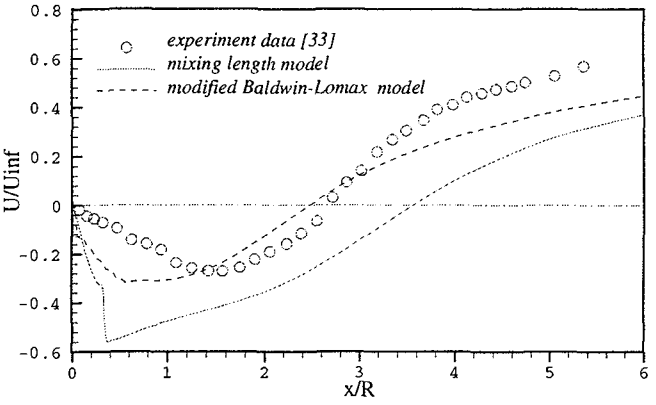

Figure 5. Mean axial velocity along cylinder centerline

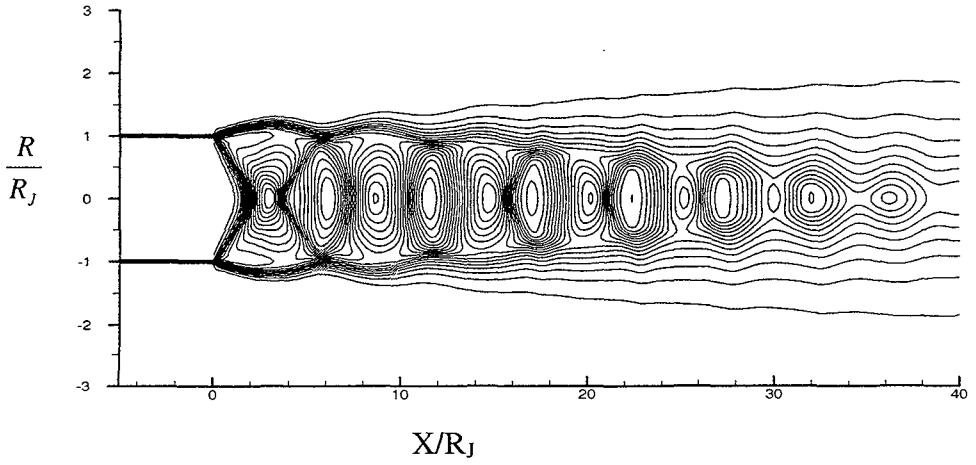

Figure 6. Density contours, k-ε model with Sarkar correction

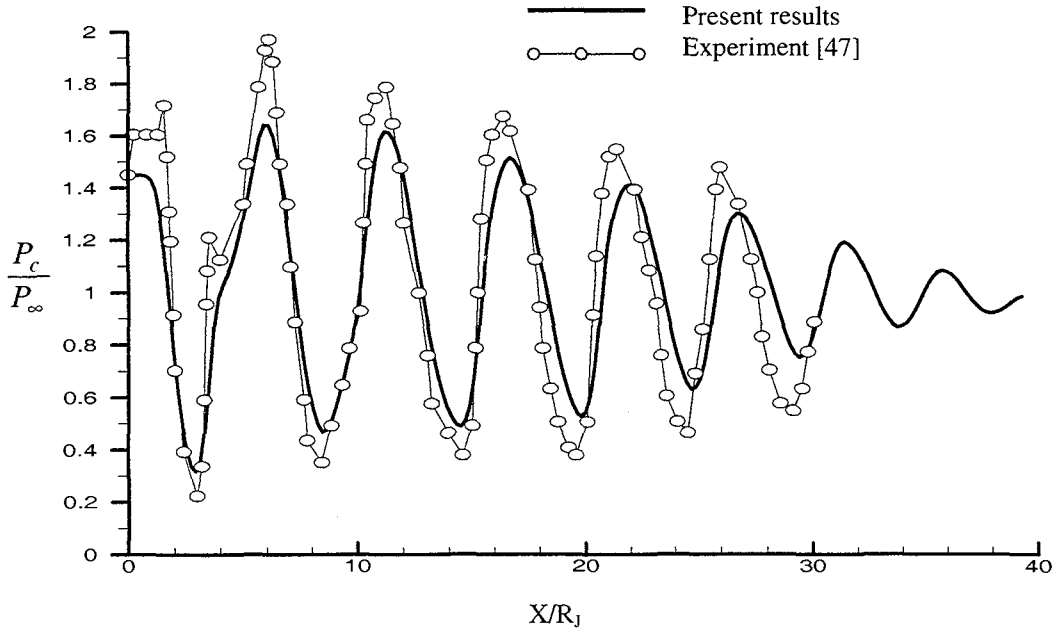

Figure 7. Centerline pressure distribution, k-ε model with Sarkar correction

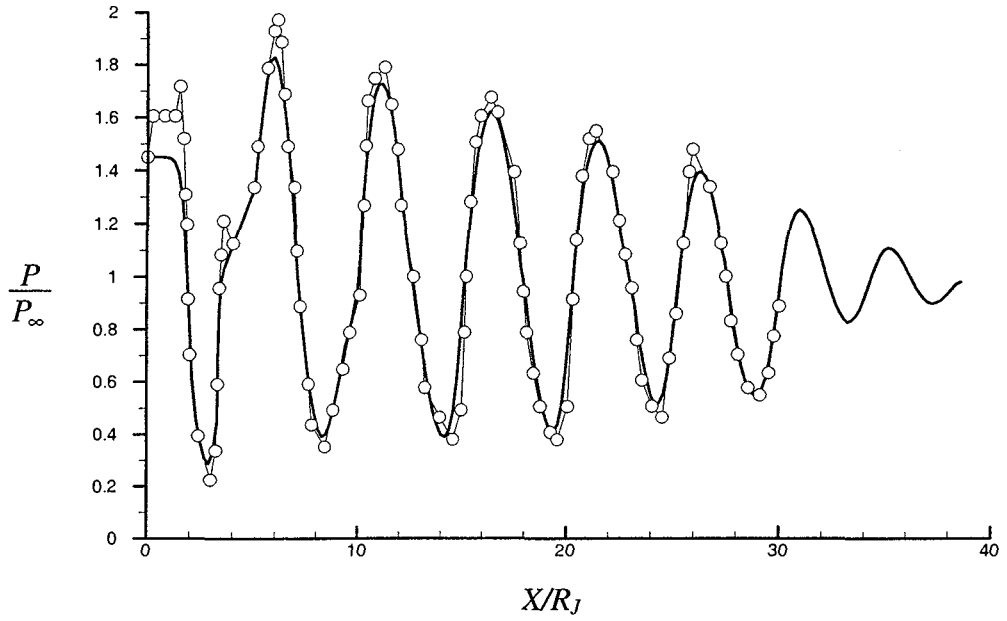

Figure 8. Centerline pressure distribution, k-ζ

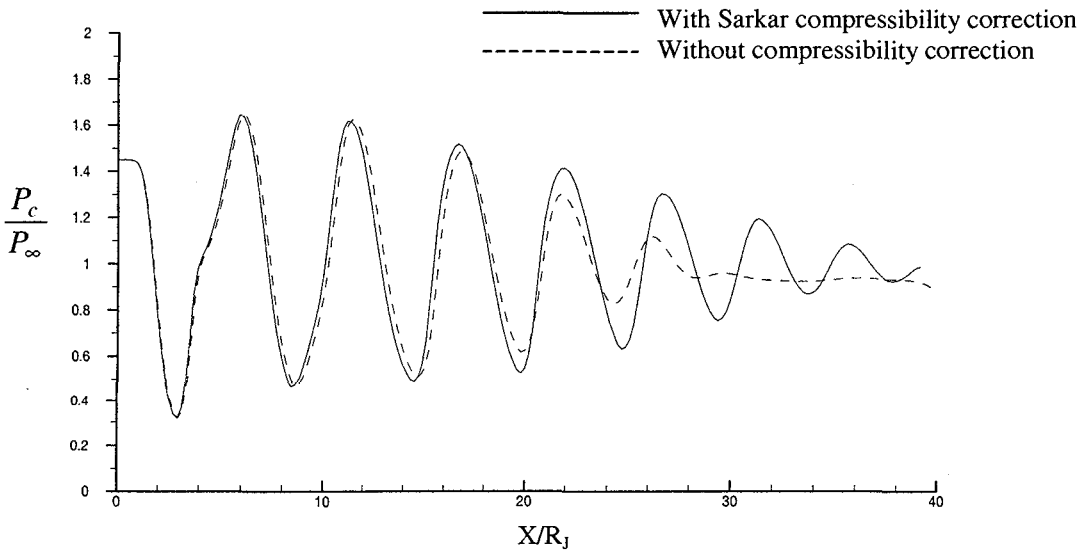

Figure 9. Centerline pressure distribution, k-ε model without and with compressibility correction

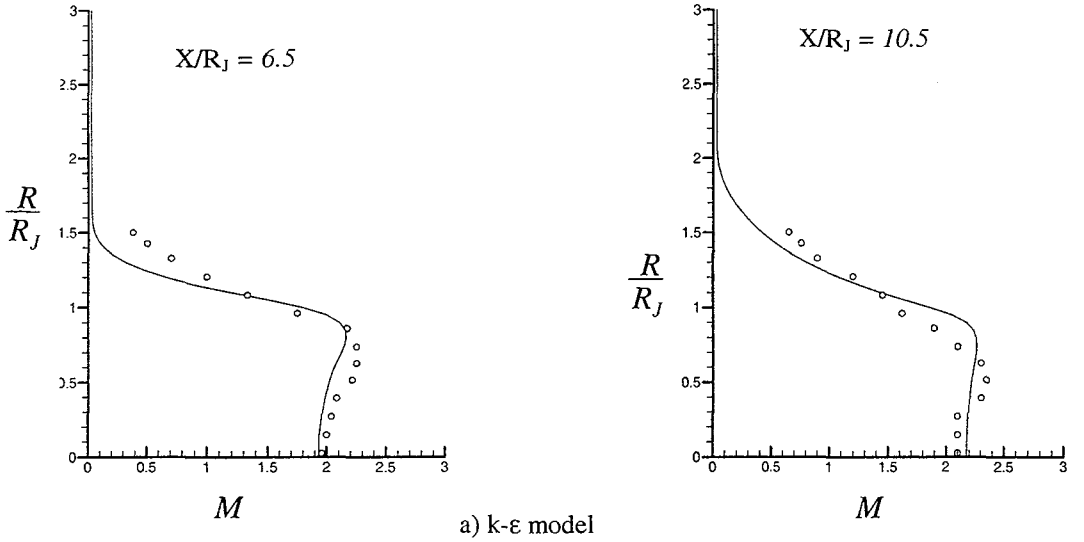

a) k-ε model

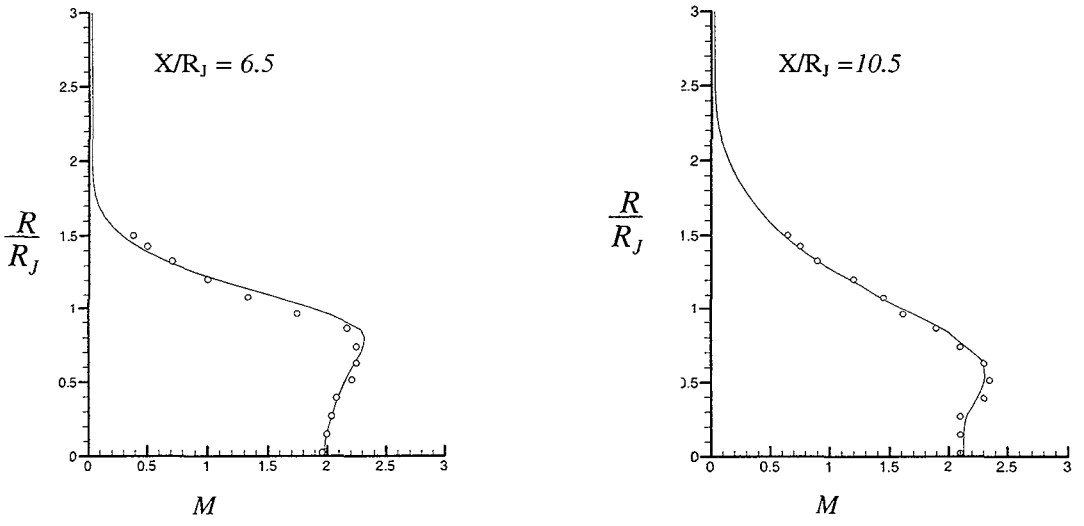

a) k-ζ model

Figure 10. Distribution of Mach number as a function of radius, k-ε and k-ζ models

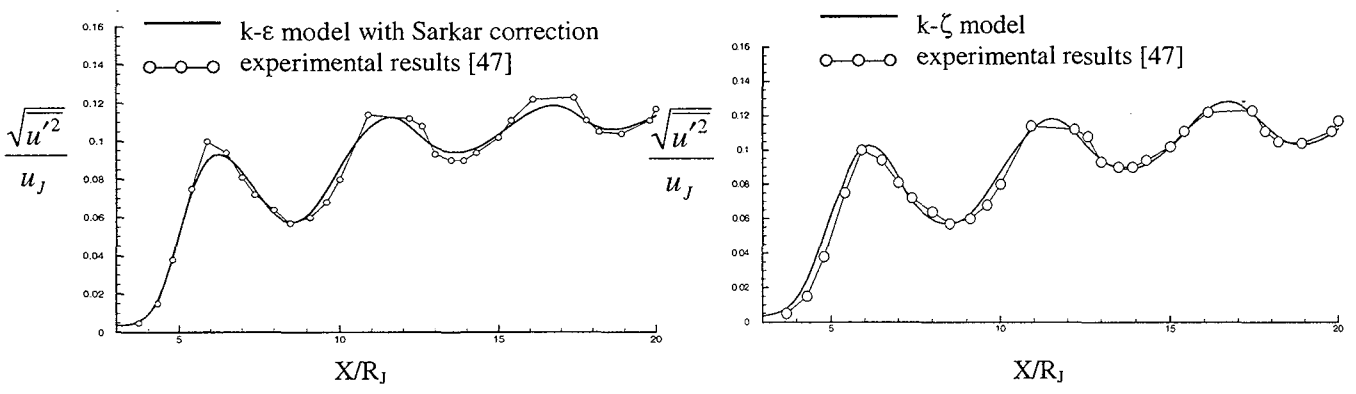

Figure 11. x-velocity component of turbulent kinetic energy intensity

M_∞	5.01
T_0, K	500
P_0, Pa	3.5×10^6
T_w, K	300
μ	Sutherland
Re, m^{-1}	4.41×10^7
Pr_t	0.9

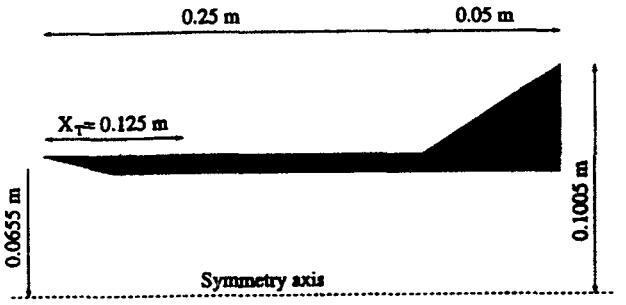

Figure 12. Geometry and inflow condition for flow over a hollow cylinder flare

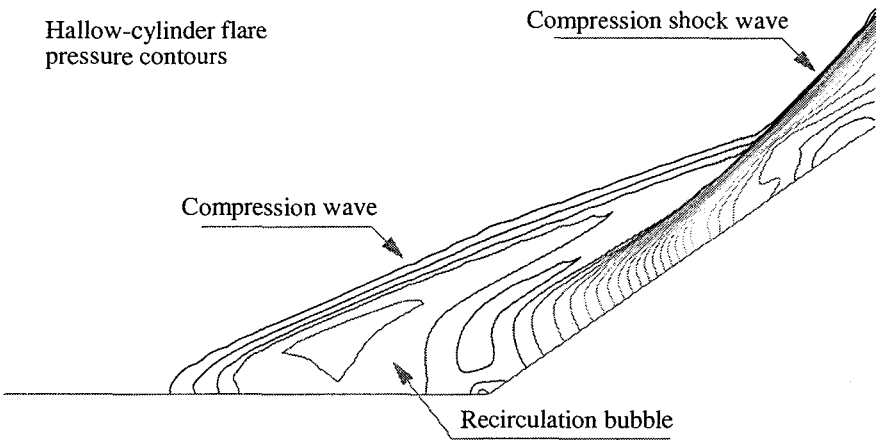

Figure 13. Pressure contours for k-l model

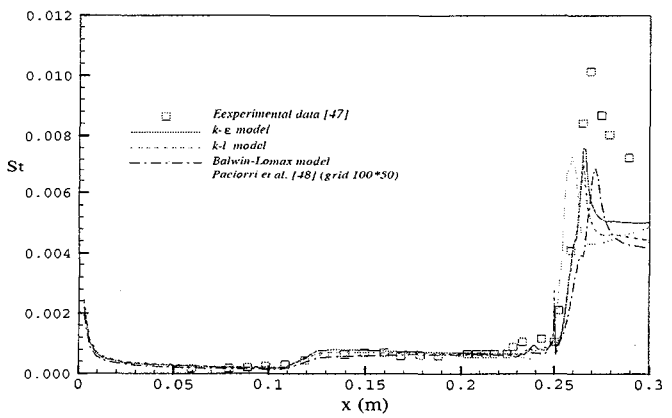

Figure 14. Wall pressure distribution

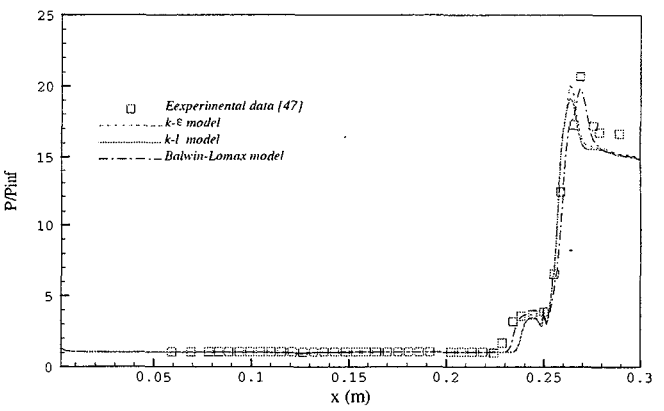

Figure 15. Stanton number